HHS Public Access

Author manuscript

Mol Psychiatry. Author manuscript; available in PMC 2018 October 03.

Published in final edited form as:

Mol Psychiatry. 2018 September ; 23(9): 1832–1850. doi:10.1038/s41380-018-0027-3.

CNTNAP2 stabilizes interneuron dendritic arbors through CASK

Ruoqi Gao, B.S.[a], **Nicolas H. Piguel, Ph.D.**[a,*], **Alexandria E. Melendez-Zaidi, Ph.D.**[a,*], **Maria Dolores Martin-de-Saavedra, Ph.D.**[a], **Sehyoun Yoon, Ph.D.**[a], **Marc P. Forrest, Ph.D.**[a], **Kristoffer Myczek, Ph.D.**[a], **Gefei Zhang, B.S.**[a], **Theron A. Russell, M.S.**[a], **John G. Csernansky, Ph.D**[b], **D. James Surmeier, Ph.D.**[a], and **Peter Penzes, Ph.D.**[a,b,1]

[a]Department of Physiology, Northwestern University Feinberg School of Medicine, Chicago, IL, 60611 USA

[b]Department of Psychiatry and Behavioral Sciences, Northwestern University Feinberg School of Medicine, Chicago, IL, 60611 USA

Abstract

Contactin associated protein-like 2 *(CNTNAP2)* has emerged as a prominent susceptibility gene implicated in multiple complex neurodevelopmental disorders, including autism spectrum disorders (ASD), intellectual disability (ID), and schizophrenia (SCZ). The presence of seizure comorbidity in many of these cases, as well as inhibitory neuron dysfunction in *Cntnap2* knockout (KO) mice, suggests CNTNAP2 may be crucial for proper inhibitory network function. However, underlying cellular mechanisms are unclear. Here we show that cultured *Cntnap2* KO mouse neurons exhibit an inhibitory neuron-specific simplification of the dendritic tree. These alterations can be replicated by acute knockdown of CNTNAP2 in mature wild-type (WT) neurons and are caused by faulty dendrite stabilization rather than outgrowth. Using structured illumination microscopy (SIM) and stimulated emission depletion microscopy (STED), two super-resolution imaging techniques, we uncovered relationships between nanoscale CNTNAP2 protein localization and dendrite arborization patterns. Employing yeast two-hybrid screening, biochemical analysis, *in situ* proximity ligation assay (PLA), SIM, and phenotype rescue, we show that these effects are mediated at the membrane by the interaction of CNTNAP2's C-terminus with calcium/calmodulin-dependent serine protein kinase (*CASK*), another ASD/ID risk gene. Finally, we show that adult *Cntnap2* KO mice have reduced interneuron dendritic length and branching, as well as decreased CASK levels in the cortical membrane fraction. Taken together, our data reveal

[1]To whom correspondence should be addressed: Peter Penzes, 303 E. Chicago Ave, WARD 7-176, Chicago, IL 60611, Tel: +1 312 503 5379; p-penzes@norhtwestern.edu.

[*]Authors contributed equally to this work

AUTHOR CONTRIBUTIONS

R.G. led the project and performed all confocal and SIM imaging experiments, K.M performed STED imaging experiments, R.G., A.E.M., S.Y., and T.A.R. performed *in vivo* experiments, R.G., N.H.P., M.P.F., and M.D.M. performed biochemistry experiments, G.Z. assisted with data analysis. P.P. supervised the project while J.G.C. and D.J.S. advised. R.G. and P.P. wrote the manuscript.

CONFLICT OF INTEREST

The authors declare no competing financial conflict of interests.

SUPPLEMENTARY INFORMATION

Supplementary information is available at Molecular Psychiatry's website.

an interneuron-specific mechanism for dendrite stabilization that may provide a cellular mechanism for inhibitory circuit dysfunction in *CNTNAP2*-related disorders.

INTRODUCTION

GABAergic interneurons comprise only 10–15% of the entire cortical neuron population but play crucial roles in fine-tuning cortical circuit function through their abilities to control excitatory neuron activity[1]. As such, interneuron dysfunction has gained a prominent role in the pathogenesis of several neurodevelopmental diseases, such as ASD, SCZ, ID, and epilepsy. Indeed, post-mortem, electrophysiological, and cellular studies have all reported inhibitory-related structural and functional perturbations in these diseases[2]. Several alterations could account for these observations, including reduced interneuron cell density, impaired input/output function, and changes in dendritic arborization. While studies on the former two are abundant[3], interneuron morphology has not been carefully studied despite its necessity for proper brain function. Dendrites determine the extent of the cell's synaptic field, impact how it processes information, and ultimately are critical determinants of neural circuit integrity[4]; conversely, abnormal dendritic architecture can impact circuit function and contribute to pathogenesis[5]. The literature, albeit scarce at this point, provides some evidence of altered interneuron morphology in some neurodevelopmental disorders, including SCZ[6], epilepsy[7], and ID[8]. Cellular knowledge about interneuron dendrite morphogenesis is equally sparse, with only a handful of molecules documented as having roles in this process[9–12].

Gene dosage, rare mutations, and common variation in *CNTNAP2* have been associated with a range of neurodevelopmental disorders, including ID[13, 14], ASD[15–19], and SCZ[20–22], with afflicted patients often sharing features of mental retardation, autistic traits, seizures, and language impairment[23]. Additionally, homozygous loss-of-function in *CNTNAP2* via compound mutations/copy number variations (CNVs) is causative for cortical dysplasia focal epilepsy (CDFE), a syndrome involving epilepsy and intellectual disability – both symptoms of chronic excitation/inhibition (E/I) imbalance[24–26]. These observations suggest that CNTNAP2 may be implicated in molecular and cellular pathways that regulate interneurons.

A role for CNTNAP2 in inhibitory neurobiological processes is supported by the presence of spontaneous seizures in *Cntnap2* KO mice beginning at 6 months[27]. Even before seizure onset, these mice show decreased GABAergic interneuron density[27], as well as alterations of synaptic function, abnormal network activity, and reduced inhibition[28–30]. Likewise, network analysis maps CNTNAP2 to modules involved in inhibitory transmission[27]. Moreover, CNTNAP2 auto-antibodies, which are present in autoimmune neurological disorders with seizures[31, 32], preferentially target inhibitory neurons[33]. While CNTNAP2 was first identified in the peripheral nervous system, where it clusters potassium channels at juxtaparanodes[34], it is also abundant in the brain and is embryonically expressed in the ganglionic eminences of the ventral telencephalon – the interneuronal birthplace[27]. These data are consistent with a role in interneuron development. Despite this, it is unclear how CNTNAP2 loss can alter inhibitory circuits.

Here we show that cultured *Cntnap2* KO mouse neurons exhibit an interneuron-specific simplification of the dendritic tree. SIM and STED super-resolution imaging techniques uncovered a novel correlation between nanoscale CNTNAP2 protein localization and dendrite arborization patterns. We show that these effects are mediated by the interaction of the CNTNAP2 C-terminus with CASK at the plasma membrane. Finally, we show that mature *Cntnap2* KO mice have reduced interneuron dendritic length/branching in specific brain regions and a decrease of CASK levels at the membrane. Our data reveal an interneuron-specific mechanism for dendrite stability mediated by the convergence between two ASD/ID risk genes, establish a previously undescribed relationship between nanoscale protein localization and dendrite architecture, and provide a cellular mechanism for inhibitory circuit dysfunction in *CNTNAP2*-related disorders.

MATERIALS AND METHODS

Antibodies and plasmids

A detailed antibody and primer list is presented in the supplementary information.

pEGFP-N2 and pmCherry-C1 plasmids were purchased from Clontech (Mountain View, CA, USA). pCS2-FLAG was purchased from Addgene (Cambridge, MA, USA, #16331). FLAG-CNTNAP2 was generated by subcloning human CNTNAP2 cDNA (from a plasmid kindly provided by Dr. Elior Peles, Weizmann Institute of Science, Israel) into the peGFP-N2 vector (restriction sites BamHI and NotI, which also excises the GFP) using the Infusion cloning system from Clontech. The FLAG sequence was then inserted downstream of the signaling peptide (amino acids 1–27) using the same technique.

Untagged CASK was generated by subcloning human CASK cDNA (Addgene #23470) into peGFP-N2 with restriction sites BamHI and NotI, while CASK-HA and CASK-FLAG were made by adding the HA and FLAG tags to the C-terminus respectively. CASK-mCherry was made by subcloning CASK cDNA into the pmCherry-C1 vector with restriction site AgeI. CASKΔPDZ was made by amplifying the cDNA upstream and downstream of the PDZ domain and ligating the pieces together (Infusion).

shRNA plasmids for *CNTNAP2* (TG510300A), *CASK* (TG516864A), and scrambled controls (TR30013) were purchased from Origene (Rockwall, MD, USA). For some knockdown experiments requiring three fluorescence channels, we replaced the turboGFP on the pGFP-V-RS vector with eGFP (restriction sites BglII and NotI). RNAi-resistant point mutations were introduced into FLAG-CNTNAP2 using QuikChange II XL Site-Directed Mutagenesis Kit (Agilent, Santa Clara, CA, USA).

For experiments where GABA staining could not be performed, we used Dlx5/6-GFP (a gift from Dr. Daniel Vogt; Michigan State University), an expression plasmid which utilizes the Dlx5/6 enhancer to selectively express GFP in interneurons[35].

Mice

All animal procedures were performed with the approval of the Institutional Animal Care and Use Committee (IACUC) at Northwestern University. *Cntnap2* KO mice (CD1) were

generated by Dr. Elior Peles. *Gad1-eGFP* mice, which selectively express GFP in a parvalbumin subset of interneurons[36], were purchased from Jackson Laboratory (Bar Harbor, ME, USA; #007677). In our hands, we did not observe this selectivity – possibly as a result of our breeding scheme (Supplementary Figure 9a) – but found all GFP cells to be GABA-positive (data not shown); we therefore focused our analysis on GABA-positive cells. All *Gad1-eGFP* Het; *Cntnap2* WT/KO mice were male and around 5 months of age.

Neuronal Culture and Transfections

High density (300 000 cells/cm^2) cortical neuron cultures were prepared from Sprague-Dawley rat E18 embryos (for shRNA, overexpression, and endogenous expression studies) or CD1 mouse P0 pups (for WT/KO and endogenous expression studies) as described previously[37]. Cortical neurons were transfected using Lipofectamine 2000 (Thermo Fisher Scientific, Waltham, MA, USA) following the manufacturer's recommendations and the neurons were maintained in the feeding media[37] for either 3 (overexpression; 24–27 *days in vitro* (DIV) for mature neurons) or 5 days (knockdown; 21–26 DIV for mature neurons or 2–7 DIV for young neurons). Any signs of poor neuronal health meant the exclusion of the cell from quantification.

Immunocytochemistry

Neurons were first washed in 0.1 M phosphate buffered saline (1× PBS) and then fixed in 4% formaldehyde-sucrose-PBS for 15 min. Fixed neurons were then permeabilized and blocked simultaneously with 5% normal goat serum (NGS) and 0.3% Triton-X-100 in 1× PBS (30 minutes at 4°C), followed by incubation of primary antibodies with 5% NGS in 1× PBS (O/N, 4°C). The coverslips were washed three times with PBS and incubated with the corresponding fluorophore-secondary antibodies with 5% NGS in 1× PBS (Alexa Fluro 488, 568, and 647; Thermo Fisher Scientific) for 1hr at 25°C. The coverslips were then washed (3x) and mounted onto slides using ProLong Antifade reagent (Invitrogen, Carlsbad, CA, USA), and stored at 4°C until the acquisition of the images.

Immunohistochemistry

Gad1-eGFP Het; *Cntnap2* WT/KO male mice at five months of age were anesthetized with Euthasol (Virbac, Fort Worth, Texas, USA) and fixed by transcardial perfusion using 4% paraformaldehyde (PFA) in 1× PBS. Brains were dissected and further incubated in 4% PFA at 25°C for 4 hours before being placed in 30% sucrose at 4°C for 3 days and frozen in OCT embedding medium (Fisher Scientific, Hampton, NH, USA). Brains were sectioned into 80 μm coronal slices (floating sections) with a cryostat, permeabilized/blocked with 3% bovine serum albumin (BSA) + 0.3% Triton X-100 in 1× PBS at 25°C for 1 hour, immunostained with GFP chicken and GABA rabbit antibodies (2 days at 4°C), followed by Alexa Fluro 488 and 568 incubation (2 days at 4°C), before being mounted onto glass slides with Dako mounting medium (Agilent) and covered with glass coverslips. Cells exhibiting intact dendritic structures were imaged (see **Confocal Microscopy Imaging**). Representative 3-D images were reconstructed with the neuTube program (neutracing.com).

Golgi Staining

The Rapid GolgiStain Kit (FD Technologies, Columbia, MD, USA) was used. Briefly, brains were dissected and immersed in impregnation solution (Solutions A+B) for 2 weeks in the dark at room temperature. The brains were then transferred into Solution C and kept for 3 days in the dark at room temperature before being flash frozen, sliced into 180 μm sections, and mounted onto gelatin-coated slides (FD Technologies). The slides were rinsed with a mixture of Solution D, E, and milli-Q water before being dehydrated with increasing concentrations (50%, 75%, 95%, and 100%) of ethanol, cleared with Xylene (Sigma), mounted using Permount (Thermo Fischer Scientific), and covered with glass coverslips. Mice (male and female) were on CD1 background and were around 6 months of age.

PLA

FLAG-CNTNAP2 and CASK-HA were overexpressed for 2–3 days in either HEK293T cells (ATCC, Manassas, VA, USA; line authenticated by company before shipment) or neurons. Coverslips were processed, fixed, and permabilized using aforementioned immunocytochemistry methods, with mouse FLAG-488 and rabbit HA-568 as primary probes (O/N, 4°C). From here, the DUOLINK kit (Sigma, St. Louis, MO, USA) was used. Briefly, mouse and rabbit PLA antibodies were used as secondary probes (37°C, 1 hr). Coverslips were then washed with Buffer A, incubated with ligase diluted in ligation solution (37°C, 30 minutes), washed again with Buffer A, and incubated with polymerase diluted in amplification solution (37°C, 100 min). The coverslips were then carefully washed with Buffer B and mounted. For PLA experiments examining endogenous CNTNAP2-CASK interactions in neurons, the same procedure was followed, except GFP was expressed for 3 days and CNTNAP2 (Millipore) and CASK (Neuromab) antibodies were used as primary probes.

Immunoprecipitation

Mouse cortex or HEK293T cells were homogenized in immunoprecipitation buffer (50 mM Tris pH 7.4, 150 mM NaCl, 0.5% Triton X-100, with protease inhibitor cocktail from Roche, Basel, Switzerland) and solubilized for 1 hour at 4°C. Solubilized material was centrifuged at 20 000 g for 10 minutes at 4°C and the supernatant was precleared with protein A/G sepharose beads (Thermo Fisher Scientific) for 30 minutes. Proteins in the precleared supernatant were then immunoprecipitated with 3 ug of antibody overnight at 4°C, followed by a 1 hour incubation with protein A/G sepharose beads the following day. Beads were then washed 3 times with IP buffer before adding 2× Laemmli buffer (Biorad, Hercules, CA, USA). Samples were analyzed by SDS-PAGE and western blotting.

Expression Time Course

Cortices from CD1 WT mice aged P0, P14, P28, 4 months, and 6 months (sex not determined at P0, P14; males for P28, 4 months, 6 months) were homogenized in immunoprecipitation buffer (50 mM Tris pH 7.4, 150 mM NaCl, 0.5% Triton X-100 with Roche protease inhibitor cocktail) and solubilized for 1 hour at 4°C. Solubilized material was centrifuged at 16 000 g for 10 minutes at 4°C and 10 ug supernatant per sample were

loaded for western blotting. For *in vitro* studies, the same procedure was performed on cultured WT rat neurons aged 7, 14, 21, and 28 DIV.

Fractionation

Subcellular fractionation was performed essentially as previously described[38]. Briefly, cortices from 6-week old mice were homogenized in cold sucrose buffer (20 mM HEPES pH 7.4, 320 mM sucrose, 5 mM EDTA) supplemented with protease inhibitor cocktail (Roche). Homogenates were centrifuged at low speed to pellet nuclei and cell debris (3 000 g for 20 min at 4°C) and the supernatant (S1) was then centrifuged at high speed (38 000 g for 30 min at 4°C) to obtain a membrane pellet (P2). P2 was re-suspended in potassium iodide buffer (20 mM HEPES pH 7.4, 1 M KI, 5 mM EDTA) to remove membrane-associated proteins (S3), and membranes were again collected by centrifugation (38 000 g for 20 min at 4°C). Membranes were washed (20 mM HEPES pH 7.4, 5 mM EDTA) and pelleted once more (S4) before solubilizing in CHAPS buffer (20 mM HEPES pH 7.4, 100 mM NaCl, 5 mM EDTA, 1% CHAPS) supplemented with protease inhibitors for 2 hr at 4°C. Solubilized membranes were clarified by centrifugation for 30 min at 100 000 g, 4°C (S5). The final CHAPS-insoluble pellet was re-suspended in SDS buffer (50mM TRIS pH 7.4, 150 mM NaCl, 1% SDS) supplemented with protease inhibitors, solubilized at 37°C for 20 mins and clarified by centrifugation (S6). For *Cntnap2* WT/KO mice (cortices from 4–6 month males) and HEK293T membrane fractionation experiments, the above fractionation procedure was performed until the P2 step. The P2 pellet (crude membrane fraction) was then resuspended with Tris buffer (50 mM Tris pH 7.4, 150 mM NaCl, 5 mM EDTA with inhibitors) before a 2× RIPA solution (50 mM Tris pH 7.4, 150 mM NaCl, 5 mM EDTA, 2% TritonX-100, 1% deoxycholate, 0.2% SDS + inhibitors) was added 1:1; similarly, the same ratio of 2× RIPA was also added to S1 (cytosolic fraction) and total homogenate. All RIPA-treated fractions were agitated for 1 hour and spun down at 16 000 g to isolate the supernatant. For western blotting, 10 ug of each sample was loaded.

Yeast Two-Hybrid Screening

Briefly, from the Matchmaker Gold Yeast Two-Hybrid manual (Clontech), CNTNAP2's C-terminal region (amino acids 1284–1331) was cloned into the bait vector (pGBKT7) and transformed into yeast. Bait-positive yeast were then mated with yeast containing cDNA (pGADT7) from a mouse brain library. Mated yeast were then plated onto double amino acid (-Leu/-Trp) dropout, Aureobasidin-A positive (A), and X-α-Gal positive (X) plates (DDO/X/A), a low stringency medium that selects for mated yeast containing both bait and prey vectors. DDO/X/A colonies that were blue, indicative of a possible interaction between bait-prey, were streaked onto quadruple amino acid (-Leu/-Trp/-His/-Ade) dropout, Aureobasidin-A positive (A), and X-α-Gal positive (X) plates (QDO/X/A), which require a genuine bait-prey interaction for growth. The blue colonies from QDO/X/A plates were isolated and plasmids sequenced.

Confocal Microscopy Imaging

Confocal images of neurons were obtained as described previously[39]. Briefly, for protein localization and expression studies, images were acquired by a Nikon (Amsterdam, Netherlands) C2 confocal microscope using a 63× oil immersion objective with numerical

aperture (NA) = 1.4 with 0.4 μm z-stacks. All images were acquired in the linear range of fluorescence intensity and the best single plane image from the stack was selected for analysis (for antibody validation analysis, z-projections were used). The acquisition parameters were kept the same for all conditions and images were analyzed using Fiji software. For *in vivo* dendritic arborization studies, images were taken with the C2 confocal using a 10× objective (NA = 0.3) with 1.0 μm z-stacks. For cultured dendrite morphological studies, images were acquired using a Zeiss (Oberkochen, Germany) Axioplan2 upright microscope. Images were taken with a 10× objective (NA = 0.3) and micrographs acquired using a Zeiss AxioCam MRM CCD camera. Dendrite arbors (*in vivo* and *in vitro*) were manually traced in Fiji. Sholl analysis was done using the Sholl plugin (Ghosh Lab), while total dendrite length and branch information were derived with Neuronstudio (Mt. Sinai School of Medicine) and analyzed with Lmeasure[40].

Structured Illuminated Microscopy (SIM) imaging and analysis

Neurons were fixed, and immunocytochemistry was performed as described above. Three-channel images were taken using a Nikon SIM microscope with a 100×1.49 NA objective (Cell Imaging Facility & Nikon Imaging Center, Northwestern University, Chicago, IL, USA) that allows a resolution range of 110–130 nm. Images were reconstructed and analyzed with Fiji as described previously[41]. For determining co-localization, Fiji's Colocalization plugin was used (Ratio: 50%, Threshold 1: 15, Threshold 2: 15, Display: 255). For analyzing puncta location, the distance from the center of the visible puncta to the closest peripheral edge of an overlay dendrite ROI was measured. To control for dendritic width variability, which can confound measurements, this value was normalized by the total dendritic width at that point and multiplied by 100 to achieve a percentage value. All SIM images were processed for background subtraction before analysis. Analysis of CNTNAP2 and CASK immunofluorescence was restricted to signal strictly within regions of interest (ROI) defined by GFP expression in individual neurons. All peripheral co-localized puncta outside of the ROI were not analyzed to exclude the possibility of presynaptic complexes confounding our calculations.

Stimulated Emission Depletion (STED) Microscopy

Super resolution images were acquired on a STED-capable Leica (Wetzlar, Germany) SP8 confocal microscope, and images were acquired with a 100× objective. Mature cortical interneurons were transfected with GFP, fixed, and stained with a CNTNAP2 antibody (Neuromab) as described previously. Alexa 488 and Alexa 594 secondary antibodies were used for GFP and CNTNAP2, respectively. An adjustable white laser was used for excitation at the optimum wavelength, and a standard confocal image was taken with the cell-fill GFP. Pulsed stimulation at 594nm and depletion laser of 775nm were simultaneously used for gated acquisition of CNTNAP2 at 594nm between 0.5 and 6 ns. In post processing, Huygens deconvolution software was used to enhance image clarity and resolution.

Bioinformatics Analysis

The list of candidate CNTNAP2-interacting proteins combined data from the BIOGRID database (via NCBI), proteomic data from published literature[42], and the yeast two-hybrid hits from this paper. The list of CASK-interacting proteins consisted of candidates from

BIND/BIOGRID/HRPD databases (via NCBI; Supplementary Table 1). A list of candidate ASD susceptibility genes was retrieved from the SFARI website (sfari.org, May 2017). A hypergeometric probability calculator was used (Geneprof.org) to determine the significance of overlap between data sets, with total gene set assumed to be 20 310 genes (Ensembl, July 2017) for all calculations.

Blinding and Statistical Analysis

Data from morphological (both *in vivo* and *in vitro*) and protein expression/localization studies were obtained and analyzed under blinded conditions (coverslip identity hidden, cells selected randomly, and raw data pooled during quantification).

Time course, fractionation (both *in vivo* and *in vitro*), immunoprecipitation, and antibody/shRNA validation experiments were not blinded. Cells of visibly poor health (i.e. blebs, broken dendrites, poor expression, etc.) were excluded from quantification. No animals were excluded from the analysis and no method of animal randomization was employed. Sample sizes, particularly for morphological studies, were on average between 30 – 60 cells to account for inherent cellular diversity. At least three animals per genotype were used for each *in vivo* experiment, which was sufficient for statistical significance.

All statistical tests were performed with GraphPad Prism (Version 7). Before analysis, data were first tested for normality with D'Agostino and Pearson in order to determine whether parametric or nonparametric tests were to be used. Tests involving symmetrical distributions (i.e. *t-test* or Mann-Whitney) were always two-sided. Post-hoc tests were always used in multiple comparison analysis. P values ≤0.05 were considered significant.

RESULTS

Mature *Cntnap2* KO neurons have an interneuron-specific deficit in dendrite arborization

While behavioral deficits of *Cntnap2* KO mice have been thoroughly characterized, the cellular and molecular substrates underlying these deficits are less clear. To gain insight into the cellular roles of CNTNAP2, we employed *Cntnap2* KO neuronal cultures. To determine the optimal time-point for analysis, we examined CNTNAP2 protein levels in WT neuronal cultures. CNTNAP2 increased over 12-fold at 4 weeks compared to 1 week (1week: 1±0.3 vs. 4weeks: 12.8±2.8; Figure 1a–b). As this suggested a prominent role for CNTNAP2 later in postnatal development, we investigated its role at 4 weeks. Because dendrites constitute the receptive fields of neurons and are altered in multiple neurodevelopmental disorders[3], we compared dendritic architecture in *Cntnap2* WT vs. KO neurons. We transiently expressed GFP and used a GABA antibody as a marker to identify interneurons (Figure 1c). We found that KO interneurons had reduced total dendritic length (WT: 2144±149.1 μm vs. KO: 1559±111.1 μm) and arborization compared to WT (Figure 1d–e) at 4 weeks. Surprisingly, pyramidal dendrites were unaffected (WT: 3269±110.8 μm vs. KO: 3307±111.7 μm; Figure 1h–i). CNTNAP2 overexpression reversed this phenotype in interneurons (KO: 1564±82.2 μm vs. KO+WT: 1938±89.7 μm; Figure 1f–g), while having no effect on pyramidal neurons (KO: 3038±121.9 μm vs. KO+WT: 2949±115.9 μm; Figure 1j–k). Consistent with this, immunofluorescence analysis with a CNTNAP2 antibody (Supplementary Figure 4c–d, f)

revealed a higher abundance of CNTNAP2 protein in inhibitory compared to excitatory neurons (Figure 1l–n), similar to a published cell-specific RNA-Seq database[43].

Such alterations in dendritic architecture could be caused by abnormal dendrite stabilization in mature neurons or impaired dendritic outgrowth in young neurons[44]. To distinguish between these alternatives, we analyzed dendrites in young neurons. We found no differences in dendrite length or arborization in inhibitory (WT: 891.8±53.7 μm vs. KO: 987.9±46.8 μm; Supplementary Figure 1a–b) or excitatory neurons (WT: 935±36.8 μm vs. KO: 880.9±38.5 μm; Supplementary Figure 1c–d) between WT and KO at this time. This suggests that absence of CNTNAP2 preferentially affects dendrite stabilization in more mature interneurons, and not dendrite outgrowth in young neurons. To further test this hypothesis, and to determine whether the effects of CNTNAP2 loss were cell-autonomous, we acutely knocked down CNTNAP2 in mature and in young interneurons using RNAi (Supplementary Figure 2). Consistent with the KO, CNTNAP2-silenced mature interneurons displayed reduced length and complexity, which was partially rescued by overexpression of RNAi-resistant CNTNAP2 (scrambled: 3206±142.6 μm vs. shCNTNAP2: 1640±134.6 μm vs. shCNTNAP2+rescue: 2286±150.6 μm; Supplementary Figure 3a–c). On the contrary, CNTNAP2 knockdown in young neurons had no effect on interneuron arborization (scrambled: 641.4±43.8 μm vs. shCNTNAP2: 685.9±52.8 μm; Supplementary Figure 3d–e). Taken together, these data suggest that CNTNAP2 has an important role in the stabilization of interneuronal dendritic arbors in later stages of postnatal development.

CNTNAP2 has spatially distinct localization patterns in inhibitory neuronal dendrites

Because of CNTNAP2's role in interneurons, we used different microscopy approaches to examine its subcellular distribution in interneuronal dendritic trees. Confocal imaging with a CNTNAP2 antibody (Supplementary Figure 4a–b, e), along with MAP2 as a dendritic marker and a GABA antibody as an interneuron marker, revealed that CNTNAP2 was abundant in punctate clusters throughout interneuronal dendrites at 27 DIV (Figure 2a). Further analysis revealed a CNTNAP2 spatial localization gradient, with puncta intensity (primary: 556.1±42.5 AU vs. secondary: 418.5±30.1 AU vs. tertiary: 377±35.2 AU; Figure 2b–c) and puncta size (primary: 0.26±0.03 μm^2 vs. secondary: 0.14±0.02 μm^2 vs. tertiary: 0.097±0.01 μm^2; Figure 2b–c) higher in primary dendrites while tapering off in secondary and tertiary branches. Meanwhile, CNTNAP2 puncta density was not affected by branch region (primary: 0.59±0.03 puncta/μm^2 vs. secondary: 0.57±0.05 puncta/μm^2 vs. tertiary: 0.56±0.07 puncta/μm^2; Figure 2b–c). This suggests that CNTNAP2 cluster size, but not number, have a dendrite order-sensitive spatial distribution.

Because of the limited resolution of confocal microscopy, we used SIM, a super-resolution technique that increases lateral resolution two-fold over confocal[45], to visualize ultrastructural profiles of CNTNAP2 distribution. We found CNTNAP2 to be frequently positioned in linear, bead-like configurations along dendrites (Figure 2d), which were not resolvable by confocal (Figure 2b). Three-dimensional reconstruction of stacked SIM images revealed these structures to be near the peripheral edge, suggesting membrane proximity (Figure 2e). To validate the existence of these structures using a different super-resolution method, we used STED microscopy, a point-scanning imaging technique that can

further enhance lateral resolution to 35 μm[46]. STED also detected CNTNAP2 nanostructures in primary dendrites indicating that they were not an artefact of SIM imaging (Figure 2f).

To determine the relationship between nanostructures and dendrite branch length, we used RNAi to knock down CNTNAP2 in mature interneurons (Supplementary Figure 2d–e) and quantitatively analyzed nanostructure distribution along multiple dendrite regions. Nanostructures were present most frequently in primary compared to secondary and tertiary branches, with RNAi strongly reducing their abundance in secondary and tertiary dendrites (scrambled: 58% primary vs. 30% secondary vs. 33.3% tertiary; shCNTNAP2: 26% primary vs. 8% secondary vs. 12% tertiary; Figure 2g–h). Analysis of RNAi-expressing interneurons also revealed a surprising stability of primary, but significant decrease of distal branch length (primary scrambled: 301.4±26.1 μm vs. primary shCNTNAP2: 398.8±36.8 μm; secondary scrambled: 838.8±57.8 μm vs. secondary shCNTNAP2: 632.5±48.3 μm; tertiary scrambled: 876.3±65.0 μm vs. tertiary shCNTNAP2: 622.9±50.7 μm; Figure 2i), which correlated with the abundance of residual nanostructures (Figure 2g–i). Taken together, these data indicate that CNTNAP2 distribution correlates with interneuronal dendrite branch stability.

CNTNAP2 interacts with CASK at the plasma membrane in cortical GABAergic interneurons

We next investigated the mechanisms of CNTNAP2-dependent dendrite stabilization. Because the effects of CNTNAP2 knockdown were cell-autonomous, and because cell adhesion molecules often utilize C-termini for intracellular signaling and protein-protein interactions[47], we performed a yeast two-hybrid screen of a mouse brain cDNA library with the entire CNTNAP2 C-terminus as bait (amino acids 1284–1331) to find intracellular interactors. We identified 41 unique clones (Supplementary Table 1) of which the scaffold protein CASK was one of the most highly represented.

We validated the interaction by co-transforming yeast with bait/prey plasmids and observed subsequent growth on high stringency plates (QDO/X/O), indicating a physical interaction (Figure 3a, Supplementary Figure 5a; black lines). We confirmed that CNTNAP2 and CASK participated in common protein complexes in native mouse brain tissue by co-immunoprecipitating and reverse co-immunoprecipitating them (Figure 3b–c). To determine the protein domains involved in their interaction, we co-expressed individual domain truncations (Supplementary Figure 5a; red lines) of CNTNAP2 with CASK in HEK293T cells and performed co-immunoprecipitations. We found the C-terminal PDZ-binding motif of CNTNAP2 interacted with CASK, as its deletion prevented CASK immunoprecipitation (Figure 3d). Conversely, deletion of CASK's PDZ domain caused a significant reduction of proximity-ligation assay (PLA) signal when co-expressed with CNTNAP2 in HEK293T cells (CNTNAP2+CASK: 0.27±0.04 μm^2 vs. CNTNAP2+CASKΔPDZ: 0.16±0.02 μm^2; Supplementary Figure 5b–c).

To determine the function of this interaction, we fractionated HEK293T cell homogenates and observed co-expression of CNTNAP2 and CASK, but not CASKΔPDZ, increased CASK in the membrane fraction (CASK: 41.1±1.9% vs. CNTNAP2+CASK: 51.8±0.7% vs. CNTNAP2+CASKΔPDZ: 35.2±2.1%), consistent with immunocytochemistry (Supplementary Figure 5b). Membrane localization was unaffected when CASK or

CASKΔPDZ were expressed alone (CASK: 44.4±1.5% vs. CASKΔPDZ: 43.3±2.3%) (Figure 3e).

We next investigated the relative spatial localization of CNTNAP2 and CASK. Confocal microscopy showed that they partially co-localized in interneuronal dendrites (Supplementary Figure 5d). To determine where the CNTNAP2 and CASK interaction was spatially localized, we imaged endogenous proteins with SIM. Co-localization occurred frequently near the lateral edge (48.1% and 45.7% of total co-localized CASK and CNTNAP2 were respectively within 10% of the peripheral edge; Figure 3f–g), suggesting CASK binds to CNTNAP2 near the plasma membrane. We validated this using PLA, which showed both molecules (Figure 3h, Supplementary Figure 5e), often interacted *in situ* near the dendrite's peripheral edge. By subcellular fractionation and salt/detergent solubilization of mouse brain homogenates (Figure 3i) we found both CNTNAP2 and CASK were highly abundant in the washed membrane fraction (S5), consistent with previous publications[48, 49]; notably, CASK was not removed from the membrane even by stringent wash conditions (see Methods). This suggests that CASK interacts with high affinity with CNTNAP2 and other transmembrane proteins. Lastly, CASK protein levels increased with age in cultured cortical neurons, in a similar pattern as CNTNAP2 (Figure 3j–k)[50], supporting functional roles later in postnatal development[51]. In summary, CNTNAP2 recruits CASK to the plasma membrane through the interaction of its C-terminal PDZ-binding motif with the PDZ domain of CASK.

CNTNAP2 regulates CASK recruitment to the plasma membrane and stability

To understand the mechanistic significance of the CNTNAP2-CASK interaction, we tested the impact of their reciprocal knockdowns on each other. CNTNAP2 knockdown resulted in a reduction of average CASK fluorescence intensity (scrambled: 1288±100.3 AU vs. shCNTNAP2: 899.6±61.8 AU) and puncta size (scrambled: 0.92±0.2 μm^2 vs. shCNTNAP2: 0.26±0.06 μm^2) in interneuronal dendrites (Figure 4a–b), and somas (scrambled: 1214±110 AU vs. shCNTNAP2: 738.9±89.9 AU; Figure 4c–d), suggesting an effect on overall CASK protein levels. On the contrary, CASK knockdown (Supplementary Figure 7e) did not affect CNTNAP2 intensity (scrambled: 793.4±91.9 AU vs. shCASK: 685.9±57.4 AU) or puncta size (scrambled: 0.33±0.03 μm^2 vs. shCASK: 0.27±0.02 μm^2) in dendrites (Figure 4e–f) or soma (scrambled: 1026±156.6 AU vs. shCASK: 906.4±106.9 AU; Figure 4g–h).

To gain further insight into the spatial distribution of CASK or CNTNAP2 upon their reciprocal knockdown, we employed SIM. Consistent with confocal imaging, CASK puncta density was decreased in shCNTNAP2 interneurons (scrambled: 1.99±0.12 puncta/μm^2 vs. shCNTNAP2: 1.41±0.10 puncta/μm^2; Figure 4j), while CNTNAP2 puncta density remained unaltered in shCASK interneurons (scrambled: 2.77±0.13 puncta/μm^2 vs. shCASK: 2.46±0.11 puncta/μm^2; Figure 4m). However, CASK puncta in shCNTNAP2 dendrites were on average closer to the peripheral edge compared to scrambled (scrambled: 22.0±0.7% vs. shCNTNAP2: 19.5±0.8% away from periphery; Figure 4i, k), due primarily to changes in localization near the plasma membrane (scrambled: 28.4% vs. shCNTNAP2: 37.5% of all puncta within 10% of periphery; Supplementary Figure 6a). Conversely, CASK knockdown did not alter CNTNAP2 distribution (scrambled: 25.8±0.6% vs. shCASK: 25.2±0.6% away

from periphery; Figure 4l, n; or near the plasma membrane, scrambled: 16.4% vs. shCASK: 17.5% of all puncta within 10% of periphery; Supplementary Figure 6b).

CASK mediates CNTNAP2-dependent interneuron dendrite stabilization

Next, we tested whether CASK functioned downstream of CNTNAP2 to regulate interneuron dendrite stability. We overexpressed CASK in mature *Cntnap2* KO neurons and analyzed the effects on both excitatory and inhibitory cell-types. Remarkably, while CASK overexpression in inhibitory KO neurons significantly increased total dendrite length (KO: 1498±84.2 μm vs. KO+CASK: 2079±110.4 μm; Figure 5a–b), it did not affect dendrite length in KO pyramidal neurons from the same coverslips (KO: 2693±84.9 μm vs. KO +CASK: 2901±98.7 μm; Figure 5c–d). Similarly, overexpression of CASK in mature CNTNAP2 knockdown neurons rescued dendrite alterations (scrambled: 3356±137.2 μm vs. shCNTNAP2: 2010±173.8 μm vs. sh+CASK: 3172±200.7μm; Supplementary Figure 7a–b), but did not alter dendrite length or complexity in WT neurons (GFP: 3345±204.4μm vs. GFP +CASK: 3014±176.5μm; Supplementary Figure 7c–d). Conversely, CASK knockdown in mature (scrambled: 2883±136μm vs. shCASK: 2467±153μm; Supplementary Figure 7e–g) but not young (scrambled: 785.4±82.6μm vs. shCASK: 871.3±78.8μm; Supplementary Figure 7h–i) interneurons resulted in simplified interneuronal arbors. Because we have shown that CASK's PDZ domain mediates its interaction with CNTNAP2 (Figure 3d–e), we examined the role of this domain on CNTNAP2-dependent dendrite stabilization. Overexpression of CASKΔPDZ in mature *Cntnap2* KO or CNTNAP2 knockdown interneurons did not fully reverse dendrite deficits, as compared to full-length CASK (KO: 1527±52.8μm vs. KO+CASK: 1919±68.0 μm vs. KO+CASKΔPDZ: 1720±68.4 μm; Figure 5e–f; shCNTNAP2: 1646±97.5 μm vs. shCNTNAP2+CASK: 2358±118.5 μm vs. shCNTNAP2+CASKΔPDZ: 1919±95.3 μm; Supplementary Figure 7j–k). In summary, these experiments indicate that CASK, through its PDZ domain, functions downstream of CNTNAP2 to mediate dendrite stabilization in interneurons.

Reduced cortical interneuron dendritic arborization and CASK mislocalization in *Cntnap2* KO mice

Finally, to validate the above findings in intact mouse brain, we analyzed brains of *Cntnap2* WT and KO mice. We first confirmed *in vivo* the age-dependent increase of CNTNAP2 (P0: 1±0.4 vs. 4 mos: 23.1±4.4) and CASK (P0: 1±0.1 vs. 4 mos: 1.9±0.1) (Supplementary Figure 8a–b). We then crossed *Cntnap2* WT and KO mice with an interneuron-specific reporter *Gad1-eGFP* transgenic line (Supplementary Figure 9a) to examine interneuron morphology *in vivo*[36]. Because recent publications have shown that *Cntnap2* KO mice develop spontaneous seizures at 6 months[27], we analyzed 5 month-old mice, an age immediately preceding seizure onset. Because adult male KO mice have documented local hypo-connectivity in the cingulate cortex and surrounding motor regions[52], we focused our analysis on the cingulate cortex/M2 areas (Supplementary Figure 10a). Confocal imaging of 80 μm slices revealed a significant difference in the total dendrite length and complexity between WT and KO interneurons in layers IV and V (WT: 877.3±44.2 μm vs. KO: 684.9±41.5 μm; Figure 5g–h). On the contrary, we found no changes in excitatory dendrite arborization in the same region (WT: 1339±71.2μm vs. KO: 1231±73.9μm; Supplementary Figure 10b–c). In parallel, we detected reduced CASK protein abundance in KO cortical

membrane fractions as compared to WT (KO:10% membrane decrease; Figure 5i–j). In summary, our data confirm *in vitro* findings and reveal inhibitory circuit architectural deficits and CASK mislocalization in adult *Cntnap2* KO mice.

DISCUSSION

Clinical[25, 26], electrophysiological[28, 29], and behavioral[27, 53] studies of CNTNAP2 have converged upon inhibitory neurons as key cellular, functional, and pathological substrates. However, the molecular mechanisms underlying these processes are not understood. Here, we show that CNTNAP2 participates in the stabilization of already-formed interneuron dendritic trees. This is at least in part, mediated by the interaction of CNTNAP2's intracellular C-terminus with CASK's PDZ domain at the plasma membrane. The spatial distribution of CNTNAP2 along the dendritic tree may have a substantial contribution to dendrite stabilization. Loss of CNTNAP2 leads to simplified dendrites on GABAergic interneurons in layer IV and V of the cingulate/M2 regions of adult mouse brain. Our data provide new insight into the regulation of interneuron dendrite stabilization by two prominent neurodevelopmental disorder risk genes.

The establishment of the dendritic tree is a complex process with several distinct steps – neurite outgrowth, dendrite extension and branching, and arbor stabilization – each governed by a unique set of cell-intrinsic and extrinsic factors[44]. While much is known about the mechanisms underlying pyramidal neuron dendrite arborization[54], far less information exists on their inhibitory counterparts. Similarly, much is known about neuron dendrite outgrowth, but relatively little about stabilization.

Here we report an inhibitory-specific, age-dependent, and cell-autonomous simplification of dendritic arbors in *Cntnap2* KO neurons. We validated these findings respectively by analyzing neighboring GABA-negative pyramidal counterparts, by experimentation in younger neurons, and by reversing the deficit with recombinant CNTNAP2. In addition, acute CNTNAP2 knockdown during a period when dendritic arbors are fully developed faithfully reproduced these observations, further supporting a role in dendrite stabilization. Finally, *in vivo* validation confirmed simplified GABAergic interneuron dendrites in adult KO mice. These data suggest CNTNAP2 plays a late-acting role in interneuronal development, which may explain why symptoms such as language regression and epilepsy have delayed emergence in some clinical cases[24, 25]. Moreover, an age-dependent destabilization of interneuronal dendrites may also provide a cellular explanation for the occurrence of abnormal IPSCs only in adult KO mice[28, 29], as changes in GABAergic morphological complexity may affect inhibitory output. Our data represent, to our knowledge, the first report of an interneuron-specific mechanism for dendrite stabilization.

Intriguingly, a previous paper by Anderson et al., 2012 reported that CNTNAP2 RNAi-mediated knockdown results in reduced arborization in pyramidal neurons[55]. Here, we used mature *Cntnap2* KO mouse neurons, a model that is more pertinent to the phenotypes observed in brain slices of KO mice, where inhibitory circuits are affected but excitatory circuits are largely unaffected[28, 29]. We have shown previously that CNTNAP2 has a role in the maintenance of dendritic spines in pyramidal neurons[39], indicating that it has different

functions at different stages of development, in different neuronal types. Importantly, all of these cell types and cellular structures have been implicated in the pathogenesis of disorders linked to CNTNAP2.

SIM and STED imaging provide superior spatial resolution compared to conventional microscopy, allowing for unprecedented insight into the neuronal nanoscale architecture[45, 46]. SIM imaging has been previously used to investigate how subcellular localizations of synaptic molecules affect spine morphology[41] and synapse remodeling[56] in pyramidal cells, but has not yet been utilized to explore dendrite regulatory mechanisms in interneurons. Here, we employed SIM and STED to establish relationships between the distribution of CNTNAP2 nanostructures and detailed dendrite architectural features of interneurons. While confocal microscopy showed CNTNAP2 to be concentrated along primary dendritic branches, super-resolution imaging resolved branch-specific “bead”-like patterns of CNTNAP2 puncta. These features are found at high abundance in primary branches, but at much lower frequencies along distal dendrites. Remarkably, acute CNTNAP2 knockdown caused a loss of peripheral “bead”-like patterns along with reduced branch length, while having relatively less effect on proximal ones, suggesting a close relationship between the spatial location of CNTNAP2 nanostructures and branch stability. This and other emerging data[41, 56] reveal that investigating the detailed subcellular localization of disease-relevant molecules may provide novel insight into their function.

Clinical findings implicate the C-terminus of CNTNAP2 – a sequence entirely conserved across human/rat/mouse species – in neurodevelopmental disorders with epilepsy comorbidity. A homozygous deletion in *CNTNAP2 (I1253X)* causing premature termination, and thus absence of the C-terminus, was found in Amish children with CDFE – a syndrome of cortical dysplasia, focal epilepsy, ID, and ASD[25]. Temporal-lobe specimens of these patients showed abnormalities of neuronal structure[25]. Deletion of the C-terminal domain was also found in several patients with epilepsy and ID[57]. Despite this, only a few intracellular protein interactors of CNTNAP2 have been characterized: the cytosolic tail is phosphorylated by protein kinase C to control protein endocytosis[58] and complexes with protein 4.1B, a cytoskeletal structural protein[59], to cluster potassium channels at the juxtaparanodes[60].

We identified a novel mechanism for intracellular function by CNTNAP2 through CASK. CASK is a multi-domain cytoskeletal scaffold found in multiple neuronal compartments, including pre-synaptic termini, dendritic spines, dendrites, and nucleus, where it coordinates signal transduction pathways at the cytoskeleton, leading to regulation of neurotransmission[61], spine maintenance[51], receptor trafficking[62], and transcription of synaptic proteins[63]. While CASK has previously been shown to co-immunoprecipitate with CNTNAP2[64], here we demonstrate that the interaction is direct and is crucial for interneuron dendrite regulation. Mechanistically, CNTNAP2 recruits and stabilizes CASK at the plasma membrane through PDZ interactions and CNTNAP2 loss leads to overall reduction and redistribution of CASK. Our data also suggest CNTNAP2 functions upstream of CASK, as manipulation of CASK abundance does not affect CNTNAP2 distribution.

It is unknown how CNTNAP2's recruitment of CASK is regulated. Utilizing available literature on Neurexin1 (a close relative of CNTNAP2) and CASK, we extrapolate that CASK and other intracellular interacting partners may compete with one another for limited binding spaces on CNTNAP2's small C-terminus[65]. Dynamic post-translational modifications on CNTNAP2's C-terminus, such as with activity-dependent phosphorylation[66], may alter its topographical landscape and affect the affinity of each interaction molecule[67]. CASK in turn may regulate dendrite morphology at the membrane through several potential mechanisms, including phosphorylation (CAM-kinase domain)[66], interactions with SAP97 (L27 domain)[68, 69], cytoskeletal binding (protein 4.1 binding site)[51], and/or nuclear translocation/transcription (GK domain)[70].

CNTNAP2 has emerged as a risk gene associated with several neurodevelopmental disorders, including ID, ASD, and epilepsy. Similarly, CASK disruption has been established to be causative for X-linked ID, nystagmus, and microcephaly with pontine and cerebellar hypoplasia[71], and is also associated with epilepsy and ASD[72, 73]. Our findings support a model whereby disease risk molecules interact directly with each other within protein-protein-interaction networks. In addition, bioinformatics analysis shows that a combined CNTNAP2-CASK interaction module became significantly enriched with psychiatric risk genes as compared to the protein-protein interaction network built around CNTNAP2 alone, using previously known direct interactors combined with our yeast two-hybrid list (Supplementary Figure 11a, Supplementary Table 1). The global output of these networks may regulate key cellular phenotypes, which when altered, result in disease with overlapping symptomatology. These results highlight the importance of looking beyond individual genes and into comprehensive mechanisms of molecular convergence. Elucidating the shared functions of newly identified disease-associated genes is a key step in the functional analysis of genetic findings.

Previous work has established conserved phenotypes indicative of inhibitory circuit dysfunction in KO models and human patients with *CNTNAP2* gene perturbations. Our findings provide a possible mechanism to explain these observations: reduced expression or damaging mutations in CNTNAP2 might interfere with interneuron dendrite stabilization, which in turn may cause greater seizure susceptibility or altered information transfer from decreased inhibitory drive and overall increased circuit excitability. In addition, abnormal interneuron dendrite stabilization may serve as a cellular convergence point in CNTNAP2/CASK pathophysiology, thus opening up new avenues of investigation on this pathway.

Supplementary Material

Refer to Web version on PubMed Central for supplementary material.

Acknowledgments

This work was supported by grants NS100785 and MH097216 from the NIH-NIMH to P.P and F30MH096457 to R.G. SIM imaging work was performed at the Northwestern University Center for Advanced Microscopy generously supported by NCI CCSG P30 CA060553 awarded to the Robert H Lurie Comprehensive Cancer Center. Structured illumination microscopy was performed on a Nikon N-SIM system, purchased through the support of NIH 1S10OD016342-01. We thank Dr. Joshua Zachary Rappoport for help with SIM imaging, Dr. Daniel Vogt for his consultation, and Xi Chao for help with figure illustrations.

References

1. Markram H, Toledo-Rodriguez M, Wang Y, Gupta A, Silberberg G, Wu C. Interneurons of the neocortical inhibitory system. Nat Rev Neurosci. 2004; 5(10):793–807. [PubMed: 15378039]
2. Marin O. Interneuron dysfunction in psychiatric disorders. Nat Rev Neurosci. 2012; 13(2):107–120. [PubMed: 22251963]
3. Gao R, Penzes P. Common mechanisms of excitatory and inhibitory imbalance in schizophrenia and autism spectrum disorders. Curr Mol Med. 2015; 15(2):146–167. [PubMed: 25732149]
4. Srivastava DP, Copits BA, Xie Z, Huda R, Jones KA, Mukherji S, et al. Afadin is required for maintenance of dendritic structure and excitatory tone. J Biol Chem. 2012; 287(43):35964–35974. [PubMed: 22948147]
5. Kulkarni VA, Firestein BL. The dendritic tree and brain disorders. Mol Cell Neurosci. 2012; 50(1): 10–20. [PubMed: 22465229]
6. Kalus P, Bondzio J, Federspiel A, Muller TJ, Zuschratter W. Cell-type specific alterations of cortical interneurons in schizophrenic patients. Neuroreport. 2002; 13(5):713–717. [PubMed: 11973476]
7. Magloczky Z, Wittner L, Borhegyi Z, Halasz P, Vajda J, Czirjak S, et al. Changes in the distribution and connectivity of interneurons in the epileptic human dentate gyrus. Neuroscience. 2000; 96(1):7–25. [PubMed: 10683405]
8. Redolfi N, Galla L, Maset A, Murru L, Savoia E, Zamparo I, et al. Oligophrenin-1 regulates number, morphology and synaptic properties of adult-born inhibitory interneurons in the olfactory bulb. Hum Mol Genet. 2016; 25(23):5198–5211. [PubMed: 27742778]
9. Cahill ME, Jones KA, Rafalovich I, Xie Z, Barros CS, Muller U, et al. Control of interneuron dendritic growth through NRG1/erbB4-mediated kalirin-7 disinhibition. Mol Psychiatry. 2012; 17(1):1–107. 99–107. [PubMed: 21483438]
10. Cobos I, Calcagnotto ME, Vilaythong AJ, Thwin MT, Noebels JL, Baraban SC, et al. Mice lacking Dlx1 show subtype-specific loss of interneurons, reduced inhibition and epilepsy. Nat Neurosci. 2005; 8(8):1059–1068. [PubMed: 16007083]
11. Gomez-Climent MA, Guirado R, Castillo-Gomez E, Varea E, Gutierrez-Mecinas M, Gilabert-Juan J, et al. The polysialylated form of the neural cell adhesion molecule (PSA-NCAM) is expressed in a subpopulation of mature cortical interneurons characterized by reduced structural features and connectivity. Cereb Cortex. 2011; 21(5):1028–1041. [PubMed: 20843898]
12. Wirth MJ, Brun A, Grabert J, Patz S, Wahle P. Accelerated dendritic development of rat cortical pyramidal cells and interneurons after biolistic transfection with BDNF and NT4/5. Development. 2003; 130(23):5827–5838. [PubMed: 14573511]
13. Zweier C, de Jong EK, Zweier M, Orrico A, Ousager LB, Collins AL, et al. CNTNAP2 and NRXN1 are mutated in autosomal-recessive Pitt-Hopkins-like mental retardation and determine the level of a common synaptic protein in Drosophila. Am J Hum Genet. 2009; 85(5):655–666. [PubMed: 19896112]
14. Sehested LT, Moller RS, Bache I, Andersen NB, Ullmann R, Tommerup N, et al. Deletion of 7q34–q36. 2 in two siblings with mental retardation, language delay, primary amenorrhea, and dysmorphic features. Am J Med Genet A. 2010; 152A(12):3115–3119. [PubMed: 21082657]
15. Bakkaloglu B, O'Roak BJ, Louvi A, Gupta AR, Abelson JF, Morgan TM, et al. Molecular cytogenetic analysis and resequencing of contactin associated protein-like 2 in autism spectrum disorders. Am J Hum Genet. 2008; 82(1):165–173. [PubMed: 18179895]
16. Rossi E, Verri AP, Patricelli MG, Destefani V, Ricca I, Vetro A, et al. A 12Mb deletion at 7q33–q35 associated with autism spectrum disorders and primary amenorrhea. Eur J Med Genet. 2008; 51(6):631–638. [PubMed: 18675947]
17. Alarcon M, Abrahams BS, Stone JL, Duvall JA, Perederiy JV, Bomar JM, et al. Linkage, association, and gene-expression analyses identify CNTNAP2 as an autism-susceptibility gene. Am J Hum Genet. 2008; 82(1):150–159. [PubMed: 18179893]
18. O'Roak BJ, Deriziotis P, Lee C, Vives L, Schwartz JJ, Girirajan S, et al. Exome sequencing in sporadic autism spectrum disorders identifies severe de novo mutations. Nat Genet. 2011; 43(6): 585–589. [PubMed: 21572417]

19. Anney R, Klei L, Pinto D, Almeida J, Bacchelli E, Baird G, et al. Individual common variants exert weak effects on the risk for autism spectrum disorders. Hum Mol Genet. 2012; 21(21):4781–4792. [PubMed: 22843504]
20. Ji W, Li T, Pan Y, Tao H, Ju K, Wen Z, et al. CNTNAP2 is significantly associated with schizophrenia and major depression in the Han Chinese population. Psychiatry Res. 2013; 207(3): 225–228. [PubMed: 23123147]
21. Friedman JI, Vrijenhoek T, Markx S, Janssen IM, van der Vliet WA, Faas BH, et al. CNTNAP2 gene dosage variation is associated with schizophrenia and epilepsy. Mol Psychiatry. 2008; 13(3): 261–266. [PubMed: 17646849]
22. Lee IS, Carvalho CM, Douvaras P, Ho SM, Hartley BJ, Zuccherato LW, et al. Characterization of molecular and cellular phenotypes associated with a heterozygous CNTNAP2 deletion using patient-derived hiPSC neural cells. NPJ schizophrenia. 2015:1.
23. Rodenas-Cuadrado P, Ho J, Vernes SC. Shining a light on CNTNAP2: complex functions to complex disorders. Eur J Hum Genet. 2014; 22(2):171–178. [PubMed: 23714751]
24. Rodenas-Cuadrado P, Pietrafusa N, Francavilla T, La Neve A, Striano P, Vernes SC. Characterisation of CASPR2 deficiency disorder--a syndrome involving autism, epilepsy and language impairment. BMC Med Genet. 2016; 17:8. [PubMed: 26843181]
25. Strauss KA, Puffenberger EG, Huentelman MJ, Gottlieb S, Dobrin SE, Parod JM, et al. Recessive symptomatic focal epilepsy and mutant contactin-associated protein-like 2. N Engl J Med. 2006; 354(13):1370–1377. [PubMed: 16571880]
26. Smogavec M, Cleall A, Hoyer J, Lederer D, Nassogne MC, Palmer EE, et al. Eight further individuals with intellectual disability and epilepsy carrying bi-allelic CNTNAP2 aberrations allow delineation of the mutational and phenotypic spectrum. J Med Genet. 2016; 53(12):820–827. [PubMed: 27439707]
27. Penagarikano O, Abrahams BS, Herman EI, Winden KD, Gdalyahu A, Dong H, et al. Absence of CNTNAP2 leads to epilepsy, neuronal migration abnormalities, and core autism-related deficits. Cell. 2011; 147(1):235–246. [PubMed: 21962519]
28. Jurgensen S, Castillo PE. Selective Dysregulation of Hippocampal Inhibition in the Mouse Lacking Autism Candidate Gene CNTNAP2. J Neurosci. 2015; 35(43):14681–14687. [PubMed: 26511255]
29. Bridi MS, Park SM, Huang S. Developmental Disruption of GABAAR-Meditated Inhibition in Cntnap2 KO Mice. eNeuro. 2017; 4(5)
30. Vogt D, Cho KKA, Shelton SM, Paul A, Huang ZJ, Sohal VS, et al. Mouse Cntnap2 and Human CNTNAP2 ASD Alleles Cell Autonomously Regulate PV+ Cortical Interneurons. Cereb Cortex. 2017:1–12.
31. Ramanathan S, Wong CH, Rahman Z, Dale RC, Fulcher D, Bleasel AF. Myoclonic status epilepticus as a presentation of caspr2 antibody-associated autoimmune encephalitis. Epileptic Disord. 2014; 16(4):477–481. [PubMed: 25497146]
32. van Sonderen A, Arino H, Petit-Pedrol M, Leypoldt F, Kortvelyessy P, Wandinger KP, et al. The clinical spectrum of Caspr2 antibody-associated disease. Neurology. 2016; 87(5):521–528. [PubMed: 27371488]
33. Pinatel D, Hivert B, Boucraut J, Saint-Martin M, Rogemond V, Zoupi L, et al. Inhibitory axons are targeted in hippocampal cell culture by anti-Caspr2 autoantibodies associated with limbic encephalitis. Front Cell Neurosci. 2015; 9:265. [PubMed: 26217189]
34. Poliak S, Salomon D, Elhanany H, Sabanay H, Kiernan B, Pevny L, et al. Juxtaparanodal clustering of Shaker-like K+ channels in myelinated axons depends on Caspr2 and TAG-1. J Cell Biol. 2003; 162(6):1149–1160. [PubMed: 12963709]
35. Fazzari P, Paternain AV, Valiente M, Pla R, Lujan R, Lloyd K, et al. Control of cortical GABA circuitry development by Nrg1 and ErbB4 signalling. Nature. 2010; 464(7293):1376–1380. [PubMed: 20393464]
36. Chattopadhyaya B, Di Cristo G, Higashiyama H, Knott GW, Kuhlman SJ, Welker E, et al. Experience and activity-dependent maturation of perisomatic GABAergic innervation in primary visual cortex during a postnatal critical period. J Neurosci. 2004; 24(43):9598–9611. [PubMed: 15509747]

37. Srivastava DP, Woolfrey KM, Penzes P. Analysis of dendritic spine morphology in cultured CNS neurons. Journal of visualized experiments : JoVE. 2011; (53):e2794. [PubMed: 21775964]
38. Nakagawa T, Cheng Y, Ramm E, Sheng M, Walz T. Structure and different conformational states of native AMPA receptor complexes. Nature. 2005; 433(7025):545–549. [PubMed: 15690046]
39. Varea O, Martin-de-Saavedra MD, Kopeikina KJ, Schurmann B, Fleming HJ, Fawcett-Patel JM, et al. Synaptic abnormalities and cytoplasmic glutamate receptor aggregates in contactin associated protein-like 2/Caspr2 knockout neurons. Proc Natl Acad Sci U S A. 2015; 112(19):6176–6181. [PubMed: 25918374]
40. Scorcioni R, Polavaram S, Ascoli GA. L-Measure: a web-accessible tool for the analysis, comparison and search of digital reconstructions of neuronal morphologies. Nat Protoc. 2008; 3(5):866–876. [PubMed: 18451794]
41. Smith KR, Kopeikina KJ, Fawcett-Patel JM, Leaderbrand K, Gao R, Schurmann B, et al. Psychiatric risk factor ANK3/ankyrin-G nanodomains regulate the structure and function of glutamatergic synapses. Neuron. 2014; 84(2):399–415. [PubMed: 25374361]
42. Chen N, Koopmans F, Gordon A, Paliukhovich I, Klaassen RV, van der Schors RC, et al. Interaction proteomics of canonical Caspr2 (CNTNAP2) reveals the presence of two Caspr2 isoforms with overlapping interactomes. Biochim Biophys Acta. 2015; 1854(7):827–833. [PubMed: 25707359]
43. Mo A, Mukamel EA, Davis FP, Luo C, Henry GL, Picard S, et al. Epigenomic Signatures of Neuronal Diversity in the Mammalian Brain. Neuron. 2015; 86(6):1369–1384. [PubMed: 26087164]
44. Scott EK, Luo L. How do dendrites take their shape? Nat Neurosci. 2001; 4(4):359–365. [PubMed: 11276225]
45. Gustafsson MG. Nonlinear structured-illumination microscopy: wide-field fluorescence imaging with theoretically unlimited resolution. Proc Natl Acad Sci U S A. 2005; 102(37):13081–13086. [PubMed: 16141335]
46. Hell SW, Wichmann J. Breaking the diffraction resolution limit by stimulated emission: stimulated-emission-depletion fluorescence microscopy. Opt Lett. 1994; 19(11):780–782. [PubMed: 19844443]
47. Cavallaro U, Dejana E. Adhesion molecule signalling: not always a sticky business. Nat Rev Mol Cell Biol. 2011; 12(3):189–197. [PubMed: 21346732]
48. Hata Y, Butz S, Sudhof TC. CASK: a novel dlg/PSD95 homolog with an N-terminal calmodulin-dependent protein kinase domain identified by interaction with neurexins. J Neurosci. 1996; 16(8): 2488–2494. [PubMed: 8786425]
49. Hsueh YP, Yang FC, Kharazia V, Naisbitt S, Cohen AR, Weinberg RJ, et al. Direct interaction of CASK/LIN-2 and syndecan heparan sulfate proteoglycan and their overlapping distribution in neuronal synapses. J Cell Biol. 1998; 142(1):139–151. [PubMed: 9660869]
50. Frese CK, Mikhaylova M, Stucchi R, Gautier V, Liu Q, Mohammed S, et al. Quantitative Map of Proteome Dynamics during Neuronal Differentiation. Cell Rep. 2017; 18(6):1527–1542. [PubMed: 28178528]
51. Chao HW, Hong CJ, Huang TN, Lin YL, Hsueh YP. SUMOylation of the MAGUK protein CASK regulates dendritic spinogenesis. J Cell Biol. 2008; 182(1):141–155. [PubMed: 18606847]
52. Liska A, Bertero A, Gomolka R, Sabbioni M, Galbusera A, Barsotti N, et al. Homozygous Loss of Autism-Risk Gene CNTNAP2 Results in Reduced Local and Long-Range Prefrontal Functional Connectivity. Cereb Cortex. 2017:1–13.
53. Selimbeyoglu A, Kim CK, Inoue M, Lee SY, Hong ASO, Kauvar I, et al. Modulation of prefrontal cortex excitation/inhibition balance rescues social behavior in CNTNAP2-deficient mice. Sci Transl Med. 2017; 9(401)
54. Jan YN, Jan LY. Branching out: mechanisms of dendritic arborization. Nat Rev Neurosci. 2010; 11(5):316–328. [PubMed: 20404840]
55. Anderson GR, Galfin T, Xu W, Aoto J, Malenka RC, Sudhof TC. Candidate autism gene screen identifies critical role for cell-adhesion molecule CASPR2 in dendritic arborization and spine development. Proc Natl Acad Sci U S A. 2012; 109(44):18120–18125. [PubMed: 23074245]

56. Yam PT, Pincus Z, Gupta GD, Bashkurov M, Charron F, Pelletier L, et al. N-cadherin relocalizes from the periphery to the center of the synapse after transient synaptic stimulation in hippocampal neurons. PLoS One. 2013; 8(11):e79679. [PubMed: 24223993]
57. Gregor A, Albrecht B, Bader I, Bijlsma EK, Ekici AB, Engels H, et al. Expanding the clinical spectrum associated with defects in CNTNAP2 and NRXN1. BMC Med Genet. 2011; 12:106. [PubMed: 21827697]
58. Bel C, Oguievetskaia K, Pitaval C, Goutebroze L, Faivre-Sarrailh C. Axonal targeting of Caspr2 in hippocampal neurons via selective somatodendritic endocytosis. J Cell Sci. 2009; 122(Pt 18): 3403–3413. [PubMed: 19706678]
59. Denisenko-Nehrbass N, Oguievetskaia K, Goutebroze L, Galvez T, Yamakawa H, Ohara O, et al. Protein 4. 1B associates with both Caspr/paranodin and Caspr2 at paranodes and juxtaparanodes of myelinated fibres. Eur J Neurosci. 2003; 17(2):411–416. [PubMed: 12542678]
60. Horresh I, Bar V, Kissil JL, Peles E. Organization of myelinated axons by Caspr and Caspr2 requires the cytoskeletal adapter protein 4. 1B. J Neurosci. 2010; 30(7):2480–2489. [PubMed: 20164332]
61. Samuels BA, Hsueh YP, Shu T, Liang H, Tseng HC, Hong CJ, et al. Cdk5 promotes synaptogenesis by regulating the subcellular distribution of the MAGUK family member CASK. Neuron. 2007; 56(5):823–837. [PubMed: 18054859]
62. Jeyifous O, Waites CL, Specht CG, Fujisawa S, Schubert M, Lin EI, et al. SAP97 and CASK mediate sorting of NMDA receptors through a previously unknown secretory pathway. Nat Neurosci. 2009; 12(8):1011–1019. [PubMed: 19620977]
63. Wang GS, Hong CJ, Yen TY, Huang HY, Ou Y, Huang TN, et al. Transcriptional modification by a CASK-interacting nucleosome assembly protein. Neuron. 2004; 42(1):113–128. [PubMed: 15066269]
64. Horresh I, Poliak S, Grant S, Bredt D, Rasband MN, Peles E. Multiple molecular interactions determine the clustering of Caspr2 and Kv1 channels in myelinated axons. J Neurosci. 2008; 28(52):14213–14222. [PubMed: 19109503]
65. Tabuchi K, Biederer T, Butz S, Sudhof TC. CASK participates in alternative tripartite complexes in which Mint 1 competes for binding with caskin 1, a novel CASK-binding protein. J Neurosci. 2002; 22(11):4264–4273. [PubMed: 12040031]
66. Mukherjee K, Sharma M, Urlaub H, Bourenkov GP, Jahn R, Sudhof TC, et al. CASK Functions as a Mg2+-independent neurexin kinase. Cell. 2008; 133(2):328–339. [PubMed: 18423203]
67. LaConte LE, Chavan V, Liang C, Willis J, Schonhense EM, Schoch S, et al. CASK stabilizes neurexin and links it to liprin-alpha in a neuronal activity-dependent manner. Cell Mol Life Sci. 2016; 73(18):3599–3621. [PubMed: 27015872]
68. Zhou W, Zhang L, Guoxiang X, Mojsilovic-Petrovic J, Takamaya K, Sattler R, et al. GluR1 controls dendrite growth through its binding partner, SAP97. J Neurosci. 2008; 28(41):10220–10233. [PubMed: 18842882]
69. Lee S, Fan S, Makarova O, Straight S, Margolis B. A novel and conserved protein-protein interaction domain of mammalian Lin-2/CASK binds and recruits SAP97 to the lateral surface of epithelia. Mol Cell Biol. 2002; 22(6):1778–1791. [PubMed: 11865057]
70. Hsueh YP, Wang TF, Yang FC, Sheng M. Nuclear translocation and transcription regulation by the membrane-associated guanylate kinase CASK/LIN-2. Nature. 2000; 404(6775):298–302. [PubMed: 10749215]
71. Moog U, Bierhals T, Brand K, Bautsch J, Biskup S, Brune T, et al. Phenotypic and molecular insights into CASK-related disorders in males. Orphanet J Rare Dis. 2015; 10:44. [PubMed: 25886057]
72. Hackett A, Tarpey PS, Licata A, Cox J, Whibley A, Boyle J, et al. CASK mutations are frequent in males and cause X-linked nystagmus and variable XLMR phenotypes. Eur J Hum Genet. 2010; 18(5):544–552. [PubMed: 20029458]
73. Lee BH, Smith T, Paciorkowski AR. Autism spectrum disorder and epilepsy: Disorders with a shared biology. Epilepsy Behav. 2015; 47:191–201. [PubMed: 25900226]

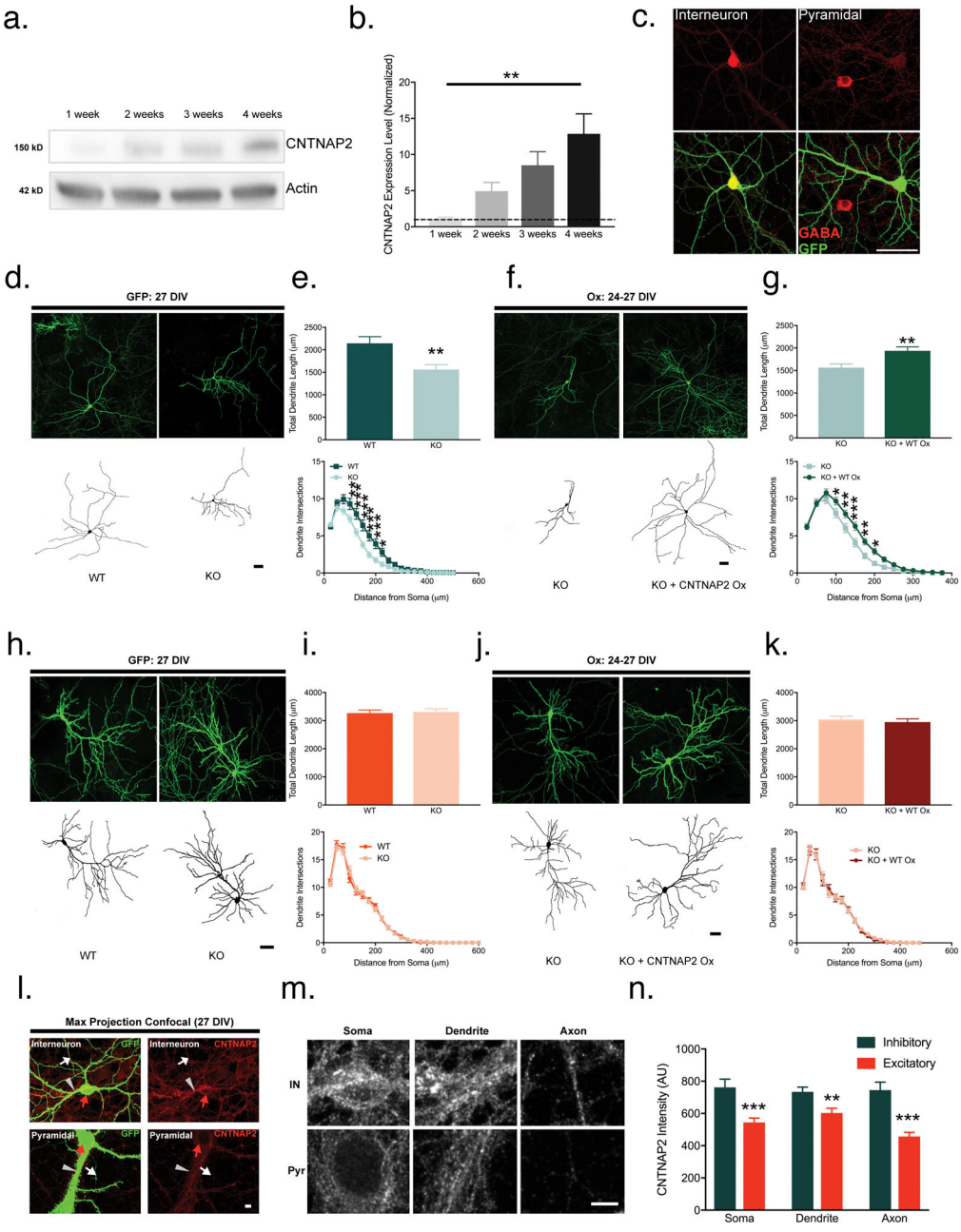

Figure 1. *Cntnap2* KO interneurons have a cell-autonomous deficit in dendrite maintenance

(a) Representative cropped western blot showing developmental time course of CNTNAP2 expression in cultured cortical neurons and (b) quantification (n = 3 independent experiments for each time point). (c) Immunostaining with a GABA antibody identifies inhibitory cells (left) but not pyramidal cells (right) (scale bar = 50 μm). (d) Representative images of GFP-expressing WT or KO mouse interneurons at 27 DIV (scale bar = 50 μm) and (e) quantification of total dendrite length and Sholl (WT: n = 43 cells from 5 cultures; KO: n = 55 cells from 6 cultures). (f) Representative images of 27 DIV KO mouse interneurons transfected (24–27 DIV) with GFP + pCS2-FLAG (KO) or GFP + FLAG-

CNTNAP2 (KO + CNTNAP2 Ox) (scale bar = 50 μm) and (g) quantification of total dendrite length and Sholl (KO: n = 49 cells from 6 cultures; KO + CNTNAP2 Ox: n = 47 cells from 6 cultures). (h) Representative images of GFP-expressing WT and KO mouse pyramidal neurons at 27 DIV (scale bar = 50 μm), with (i) quantification of total dendrite length and Sholl (WT: n = 49 cells from 6 cultures; KO: n = 50 cells from 6 cultures). (j) Representative images of 27 DIV KO mouse pyramidal cells transfected (24–27 DIV) with GFP + pCS2-FLAG (KO) or GFP + FLAG-CNTNAP2 (KO + CNTNAP2 Ox) (scale bar = 50 μm) and (k) quantification (KO: n = 36 cells from 5 cultures; KO + CNTNAP2 Ox: n = 30 cells from 5 cultures). (l) Representative images (scale bar = 5 μm) of GFP-transfected inhibitory and excitatory WT mouse neurons at 27 DIV, with soma (red arrow), dendrites (arrowhead), and axons (white arrow) highlighted. (m) Magnification of structures from (l) (scale bar = 5 μm) and (n) respective quantification (Inhibitory: n = 22 somas, 37 dendrites, and 19 axons from 3 cultures; Excitatory: n = 19 somas, 29 dendrites, and 13 axons from 3 cultures). Values are means ± SEM. * P≤0.05, ** P ≤0.01, *** P ≤0.001; one-way ANOVA with Bonferroni's correction (b), Student's *t-test* (n, total dendrite length; k), Mann-Whitney test (total dendrite length; e, g, i), and two-way ANOVA with Bonferroni's correction (Sholl; e, g, i, k).

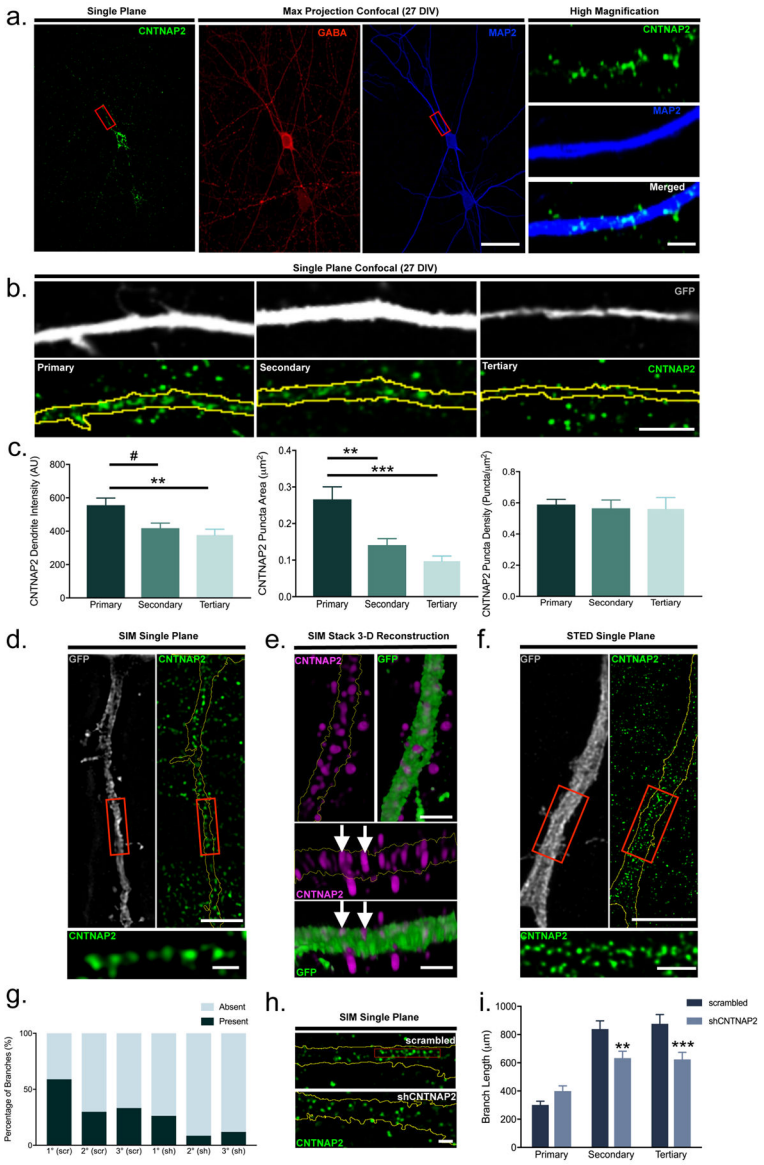

Figure 2. CNTNAP2 has spatially distinct localization patterns in inhibitory neuronal dendrites

(a) Confocal images of GABA-positive rat interneurons at 27 DIV co-stained with endogenous CNTNAP2 and the dendrite marker MAP2 (scale bar = 50 μm). Inset shows magnification of region around red box. (Scale bar = 5 μm). (b) Confocal imaging reveals general CNTNAP2 expression patterns in GFP-transfected primary, secondary, and tertiary dendritic branches (scale bar = 5 μm), with (c) quantification of intensity, puncta area, and puncta density (intensity: n = 28 primary, 28 secondary, and 25 tertiary branches from 4 cultures; puncta area/density: n = 20 primary, 20 secondary, and 18 tertiary branches from 3 cultures). (d) High resolution SIM imaging detects the presence of linear “bead”-like CNTNAP2 nanostructures in GFP-expressing dendrites of rat interneurons. Inset shows magnification of region around red box (scale bar = 5 μm and 1 μm respectively). (e) Top and side angles of a 3D reconstructed SIM image stack showing CNTNAP2 “beads” either alone or with GFP overlay (scale bars = 1 μm). White arrows point to nanostructures near

the membrane surface. (f) STED imaging confirms CNTNAP2 nanostructures in interneuron primary dendrites, with inset showing magnification of region around the red box (scale bar = 5 μm and 1 μm respectively). (g) CNTNAP2 nanostructure distribution in primary, secondary, and tertiary dendrites in mature scrambled or shCNTNAP2-treated (21–26 DIV) rat interneurons (scrambled: n = 39 primary branches, 40 secondary branches, and 36 tertiary branches from 3 cultures; shCNTNAP2: n = 38 primary branches, 35 secondary branches, and 25 tertiary branches from 3 cultures). (h) Representative SIM images of CNTNAP2 endogenous staining in scrambled or shCNTNAP2-treated rat interneuron branches (scale bar = 1 μm). (i) Quantification of primary, secondary, and tertiary branch lengths in scrambled or shCNTNAP2-treated (21–26 DIV) mature rat interneurons (scrambled: n = 57 cells from 5 cultures; shCNTNAP2: n = 68 cells from 5 cultures). Values are means ± SEM. # P=0.07, ** P≤0.01, *** P≤0.001; Kruskal-Wallis test with Dunn's correction (intensity and puncta size; c), one way-ANOVA with Bonferroni's correction (puncta density; c), two-way ANOVA with Bonferroni's correction (i).

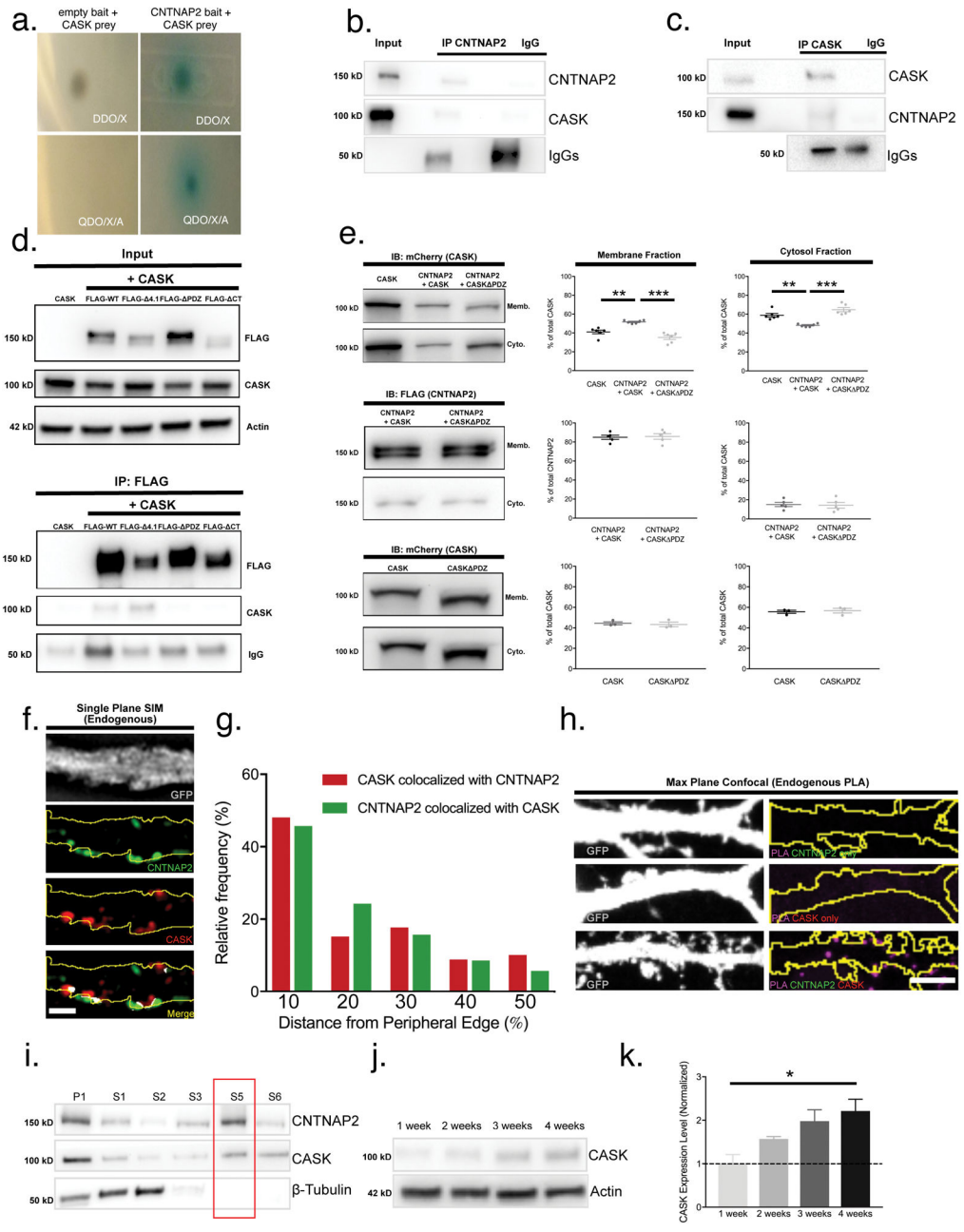

Figure 3. CNTNAP2 interacts with CASK at the plasma membrane in cortical GABAergic interneurons

(a) Only yeast cells co-expressing CNTNAP2 bait and CASK prey constructs grow on high stringency yeast plates (QDO/X/A). (b–c) Cropped western blots of co-immunoprecipitation experiments with CASK and CNTNAP2 in mouse cortex. (d) Cropped western blots showing co-immunoprecipitation of various FLAG-CNTNAP2 truncation mutants (Supplementary Figure 5a; red lines) with untagged, full-length CASK in HEK293T cells. (e) Representative cropped western blots of membrane/cytosol fractions of HEK293T cells expressing pCS2-FLAG + CASK-mCherry (CASK), FLAG-CNTNAP2 + CASK-mCherry (CNTNAP2 + CASK), or FLAG-CNTNAP2 + CASKΔPDZ-mCherry (CNTNAP2 +

CASKΔPDZ) and subsequent quantification of protein localization (CASK vs. CNTNAP2 + CASK vs. CNTNAP2 + CASKΔPDZ: 6 independent experiments; CASK alone vs. CASKΔPDZ alone: 3 independent experiments). Percentages were calculated by dividing the densitometry value of CASK/CNTNAP2 in either membrane or cytosol fraction by the summation of both. (f) Representative SIM image of endogenous CNTNAP2 and CASK co-localization (white) on a GFP-transfected interneuronal dendrite (scale bar = 5 μm). (g) Histogram showing distribution of CASK/CNTNAP2 co-localized puncta relative to the dendrite's lateral edge from (f) (CASK colocalized with CNTNAP2: n = 79 puncta from 3 cultures; CNTNAP2 colocalized with CASK: n = 70 puncta from 3 cultures). (h) Representative confocal image showing PLA signal from endogenous CASK/CNTNAP2 staining, which occurs only when CASK and CNTNAP2 primary antibodies are both applied (scale bar = 1 μm). (i) Cropped immunoblots of subcellular fractionations from adult mouse forebrain probed with CNTNAP2, CASK, and β-tubulin. CNTNAP2 and CASK, but not β-tubulin, are found in the washed membrane fraction (S5; red box). (j) Cropped western blot of time course and (k) quantification of CASK expression in cultured cortical neurons (n = 3 independent experiments). Values are means ± SEM. * P≤0.05, ** P≤0.01, *** P≤0.001; one-way ANOVA with Bonferroni's correction (k, top graph; e). Student's *t-test* (middle and bottom graphs; e).

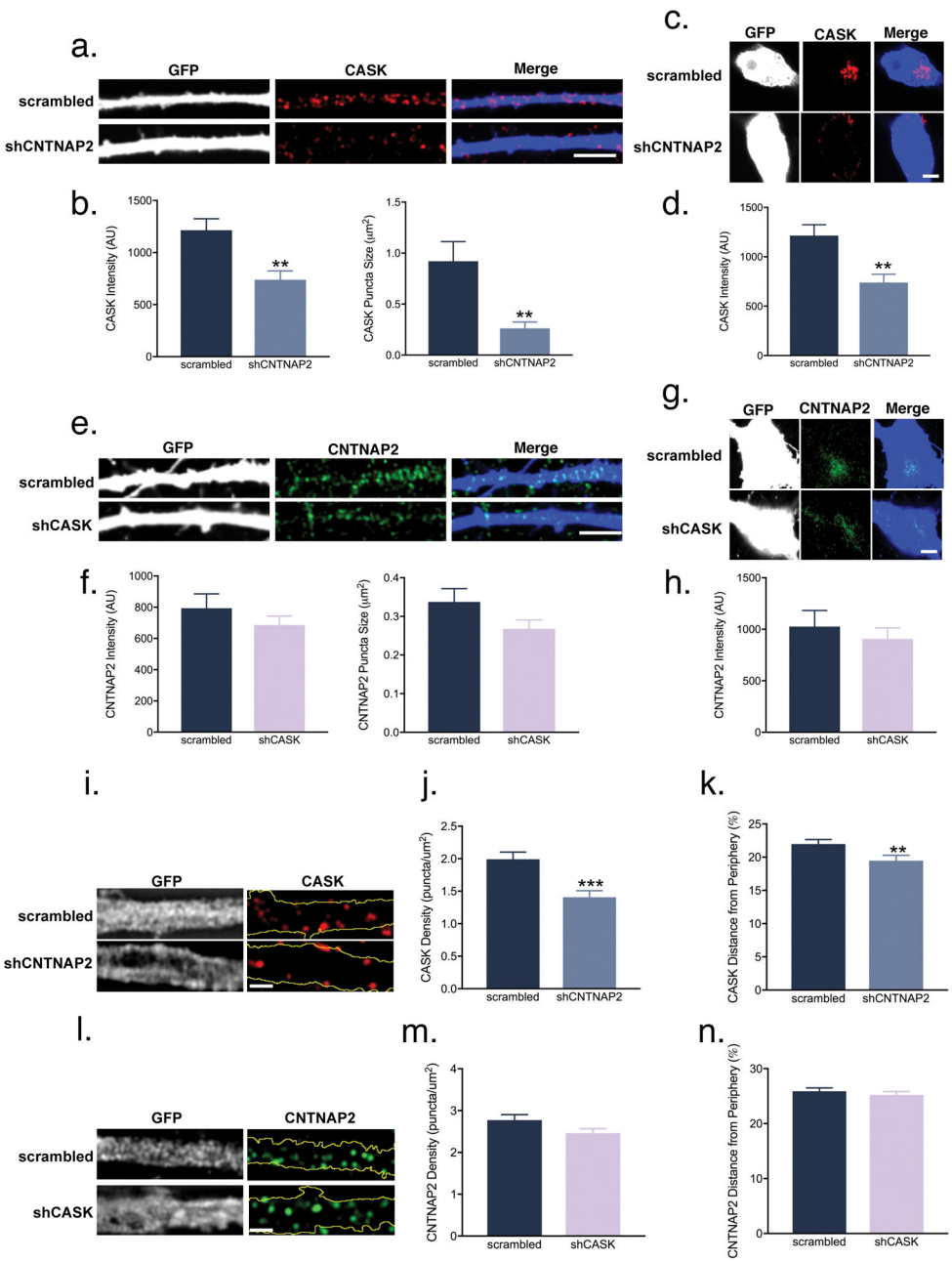

Figure 4. CNTNAP2 regulates CASK recruitment to the plasma membrane and stability

(a) Representative confocal images and (b) quantification of CASK average intensity and puncta area in scrambled or shCNTNAP2-treated (21–26 DIV) rat interneuron dendrites at 26 DIV (scale bar = 5 μm; scrambled: n = 42 branches for intensity and n = 37 branches for puncta area from 3 cultures; shCNTNAP2: n = 43 branches for intensity and n = 37 branches for puncta area from 3 cultures). (c) Representative confocal images and (d) quantification of CASK average intensity in scrambled or shCNTNAP2 interneuron somas (scale bar = 5 μm; scrambled: n = 23 cells from 3 cultures; shCNTNAP2: n = 24 cells from 3 cultures). (e) Representative confocal images and (f) quantification of CNTNAP2 average intensity and

puncta area in scrambled or shCASK-treated (21–26 DIV) rat interneuron dendrites at 26 DIV (scale bar = 5 μm; scrambled: n = 49 branches for intensity and n = 57 branches for puncta area from 4 cultures; shCASK: n = 52 branches for intensity and n = 47 branches for puncta area from 4 cultures) and (g–h) quantification of average CNTNAP2 intensity in the somas of scrambled or shCASK interneurons (scale bar = 5 μm; scrambled: n = 24 cells from 4 cultures; shCASK: n = 29 cells from 4 cultures). (i) High resolution SIM images of endogenous CASK in scrambled or shCNTNAP2 interneuron dendrites at 26 DIV (scale bar = 1 μm). (j) Analysis of CASK puncta density (scrambled: n = 31 branches from 5 cultures; shCNTNAP2: n = 26 branches from 5 cultures) and (k) average distance from peripheral edge (scrambled: n = 426 puncta from 5 cultures; shCNTNAP2: n = 306 puncta from 5 cultures) via SIM in scrambled or shCNTNAP2 interneurons. (l) High resolution SIM images of endogenous CNTNAP2 in scrambled or shCASK interneuron dendrites at 26 DIV. (m) Analysis of CNTNAP2 puncta density (scrambled: n = 23 branches from 3 cultures; shCASK: n = 25 branches from 3 cultures) and (n) average distance from peripheral edge (scrambled: n = 475 puncta from 3 cultures; shCASK: n = 473 puncta from 3 cultures) via SIM in scrambled or shCASK interneurons. Distances in (k) and (n) are measured by a percentage value, which represents the distance of the puncta's center to the closet peripheral edge divided by the total width of the dendrite at that point multiplied by 100. Values are means ± SEM. **P≤0.01, ***P≤0.001; Mann-Whitney test (b, d, f, h, k, m, n), Student's *t-test* (j).

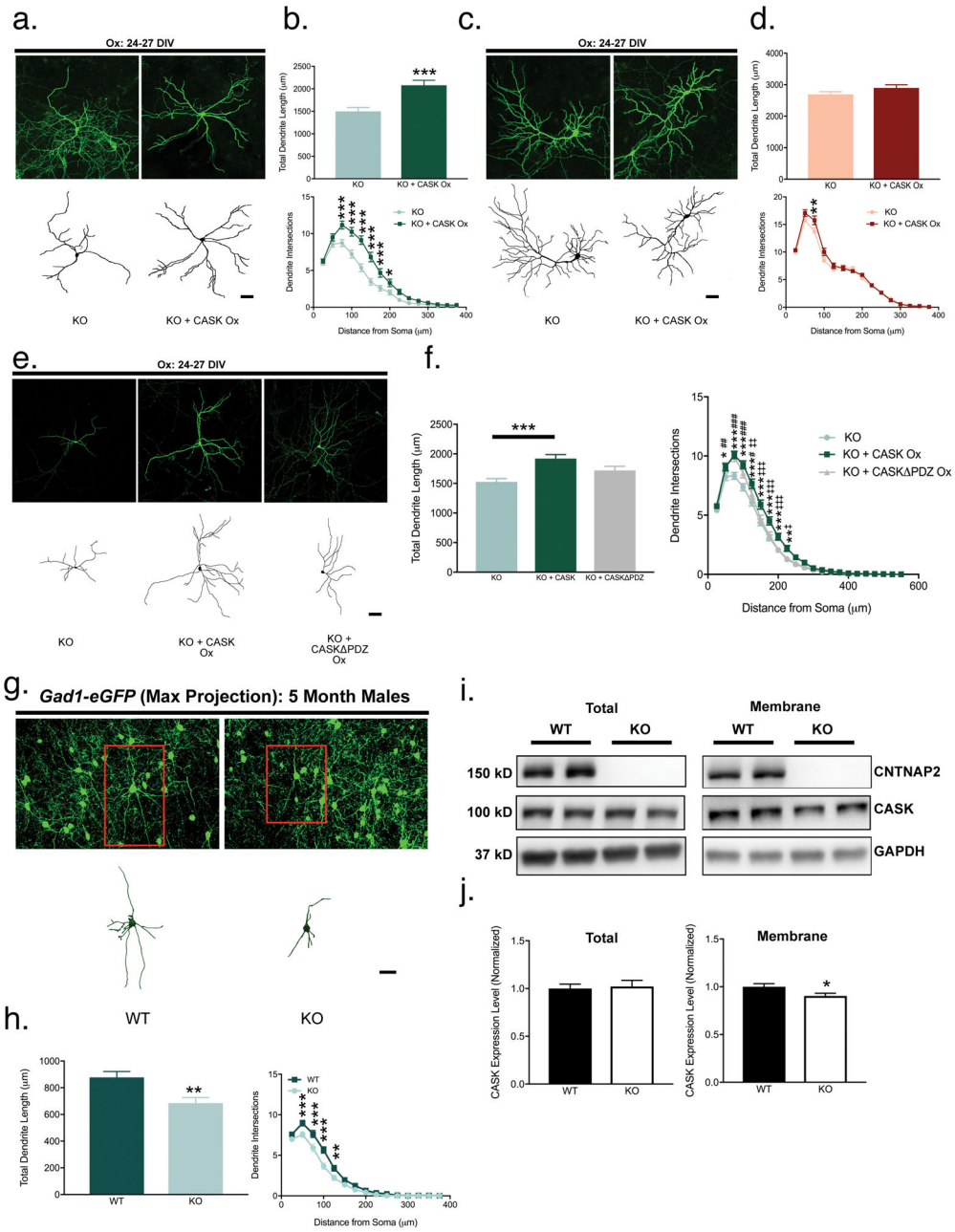

Figure 5. CASK mediates CNTNAP2-dependent interneuron dendrite stabilization and *Cntnap2* KO mice have reduced cortical interneuron dendrite arborization and CASK mislocalization

(a) Representative images of 27 DIV KO mouse interneurons transfected (24–27 DIV) with either GFP + mCherry (KO) or GFP + CASK-mCherry (KO + CASK Ox) (scale bar = 50 μm) and (b) respective quantification of total dendrite length and Sholl (KO: n = 57 cells from 4 cultures; KO + CASK Ox: 50 cells from 4 cultures). (c) Representation and (d) analysis of KO mouse pyramidal cells under the same conditions (scale bar = 50 μm; KO and KO + CASK Ox: n = 49 cells from 3 cultures). (e) Representative confocal images of 27 DIV KO mouse interneurons transfected (24–27 DIV) with GFP + mCherry (KO), GFP + CASK-mCherry (KO + CASK Ox), or GFP + CASKΔPDZ-mCherry (KO + CASKΔPDZ

Ox) (scale bar = 50 μm). (f) Quantification of (e) using total dendrite length and Sholl (KO: n = 163 cells from 10 cultures; KO + CASK Ox: n = 144 cells from 10 cultures; KO + CASKΔPDZ Ox: n = 130 cells from 10 cultures; for Sholl, * compares KO vs KO + CASK Ox, # compares KO vs. KO + CASKΔPDZ Ox and ‡ compares KO + CASK Ox vs. KO + CASKΔPDZ Ox). (g) Representative and 3-D reconstructed images of interneurons *in vivo* from layers IV and V of M2 and Cingulate Cortex in 5-month old male *Gad1-GFP* Het; *Cntnap2* WT/KO mice (scale bars = 50 μm) and (h) quantification of total dendrite length and Sholl (WT: n = 55 cells from 3 mice; KO: n = 51 cells from 3 mice). (i) Representative cropped western blots showing CASK levels in *Cntnap2* WT/KO cortical total homogenate and crude membrane fraction. GAPDH was used as a marker to determine membrane fractionation efficiency. (j) Quantification of (i) (total: n = 12 brains per genotype; membrane: n = 13 brains per genotype). Values are means ± SEM; * P≤0.05, ** P≤0.01, *** P≤0.001 (also applies for # and ‡); Mann-Whitney test (total homogenate; j, total dendrite length; b, h), Student's *t-test* (membrane fraction; j, total dendrite length; d), Kruskal-Wallis test with Dunn's correction (total dendrite length; f), Two-way ANOVA with Bonferroni's correction (Sholl; b, d, f, h).